RESEARCH ARTICLE | OCTOBER 14 2025

Thermoelectric fingerprinting of Bloch- and Néel-type skyrmions

Christopher E. A. Barker ⁽¹⁾; Elias Saugar ⁽¹⁾; Katharina Zeissler ⁽¹⁾; Robert Puttock ⁽¹⁾; Petr Klapetek ⁽¹⁾; Olga Kazakova ⁽¹⁾; Christopher H. Marrows ⁽²⁾ ⁽¹⁾; Oksana Chubykalo-Fesenko ⁽¹⁾; Craig Barton ⁽²⁾



Appl. Phys. Lett. 127, 152405 (2025) https://doi.org/10.1063/5.0284384





Articles You May Be Interested In

Magnetization reversal signatures of hybrid and pure Néel skyrmions in thin film multilayers

APL Mater. (November 2020)

Nanoscale Thermal and Thermoelectric Mapping of Semiconductor Devices and Interconnects

AIP Conf. Proc. (September 2003)

Invited Review Article: Microwave spectroscopy based on scanning thermal microscopy: Resolution in the nanometer range

Rev. Sci. Instrum. (April 2008)





Thermoelectric fingerprinting of Bloch- and Néel-type skyrmions

Cite as: Appl. Phys. Lett. **127**, 152405 (2025); doi: 10.1063/5.0284384 Submitted: 7 June 2025 · Accepted: 18 September 2025 · Published Online: 14 October 2025









AFFILIATIONS

- National Physical Laboratory, Hampton Road, Teddington TW11 OLW, United Kingdom
- ²Instituto de Ciencia de Materiales de Madrid, ICMM-CSIC, Campus de Cantoblanco, C. Sor Juana Inés de la Cruz,
- 3, Madrid 28049, Spain
- School of Physics and Astronomy, University of Leeds, Leeds LS2 9JT, United Kingdom
- ⁴Bragg Centre for Materials Research, University of Leeds, Leeds LS2 9JT, United Kingdom
- ⁵Czech Metrology Institute, Okruzni 772/31, Brno 10135, Czech Republic
- ⁶Central European Institute of Technology (CEITEC), Brno University of Technology, Purkynova 123, Brno 612 00, Czech Republic
- 7 Department of Electrical and Electronic Engineering, University of Manchester, Manchester M13 9PL, United Kingdom
- a) Electronic mail: christopher.barker@npl.co.uk
- ^{b)}Authors to whom correspondence should be addressed: C.H.Marrows@leeds.ac.uk and craig.barton@npl.co.uk

ABSTRACT

Magnetic skyrmions are nanoscale spin textures that exhibit topological stability, which, along with their thermal and electrical transport properties, make them the ideal candidates for a variety of technological applications. Accessing the skyrmion spin texture at the nanoscale and understanding its interaction with local thermal gradients is essential for engineering skyrmion-based transport phenomena. However, direct experimental insight into the local thermoelectric response of single skyrmions remains limited. To address this, we employ scanning thermoelectric microscopy (SThEM) to probe the nanoscale thermoelectric response from a single skyrmion. By mapping the local thermoelectric voltage with nanoscale precision, we reveal a unique spatially resolved response that is the convolution of the underlying spin texture of the skyrmion and its interaction with the highly localized thermal gradient originating from the heated probe. We combine this with thermoelectric modelling of a range of skyrmion spin textures to reveal unique thermoelectric responses and allow the possibility of SThEM to be used as a tool to distinguish nanoscale spin textures. These findings provide fundamental insights into the interaction of topologically protected spin textures with local thermal gradients and the resultant spin transport. We demonstrate a route to thermally characterize nanoscale spin textures, accelerating the material optimization cycle, while also opening the possibility to harness skyrmions for spin caloritronics.

© 2025 Author(s). All article content, except where otherwise noted, is licensed under a Creative Commons Attribution (CC BY) license (https://creativecommons.org/licenses/by/4.0/). https://doi.org/10.1063/5.0284384

Magnetic skyrmions are topologically protected spin textures that can emerge in chiral magnetic systems due to the interplay between the Dzyaloshinskii–Moryia interaction (DMI), perpendicular magnetic anisotropy, exchange interactions, and external magnetic fields. ¹⁻⁹ Materials with these nanoscale spin textures ^{10–12} exhibit unique electrical transport properties, such as the topological Hall effect. ^{13,14} Furthermore, owing to their strong coupling to spin currents and Rashba interfaces, current driven motion can occur at very low current densities. ^{3,15–19} These properties make them exciting candidates for a future generation of spintronic based logic and storage technologies. ²⁰ Furthermore, they are also

attractive candidates for non-von Neumann computational paradigms such as neuromorphic computing.²¹ The local spin texture plays a fundamental role in governing skyrmion dynamics, interactions, and their response to external stimuli such as electric fields,²² currents, ^{14,23} and thermal gradients.^{24,25} Understanding the nanoscale spin structure is crucial for controlling skyrmion-based transport phenomena, including the interplay between spin–orbit effects,¹⁵ their thermoelectric response,²⁶ and magnon-mediated transport.²⁷ Hence, the ability to understand and measure the local spin texture is of great importance, both from a fundamental perspective and also to optimize device performance

during material development, creating a route to expedite the *lab-to-fab* development of next generation skyrmion devices.

Probing the local properties of nanoscale spin textures requires high-resolution microscopy techniques capable of detecting their local electronic, magnetic, or—as in our work—thermoelectric responses. There have been significant developments in the real-space characterization of nanoscale spin textures, where a range of measurement solutions are available to ascertain the local magnetization with remarkable precision and sensitivity. These techniques include x-ray magnetic nanotomography, Lorentz transmission electron microscopy (LTEM), spin-polarized scanning tunneling microscopy (SPSTM), scanning probe nitrogen-vacancy (NV) magnetometry, and magnetic force microscopy (MFM). 10,28-39 More recently, scanning thermoelectric microscopy (SThEM) has emerged as powerful technique to map the various local thermoelectric responses with nanometer resolution, enabling direct investigation of the coupling between spin textures and thermal gradients, 40-47 providing an invaluable tool to study spin caloritronic effects at the nanoscale. 48-50 In this work, we employ SThEM to measure the thermoelectric signature of an individual skyrmion, providing insight into the fundamental interactions that govern skyrmionic thermoelectric effects at the nanoscale. A combination of experimental and thermoelectric modelling is used to distinguish the signal resulting from two skyrmion types: Bloch and Néel. Our findings provide the foundations to ascertain the local real-space magnetization of topological spin textures using a generic lab-based scanning probe microscope and, more fundamentally, offer a route to explore thermally driven charge, spin, and thermal (magnon) transport in complex magnetic spin textures at the nanoscale.

Figure 1(a) schematically shows the SThEM experimental setup, detailing how a constant-current Joule heated (ThermaLeverTM) scanning probe, operated in the contact mode, is used to introduce a nanometric thermal gradient. Electrical readout was achieved using a Keysight 34420A nanovoltmeter, which was synced to the scanning probe microscopes controller, such that the electrical readout could be mapped spatially with the sample topography. ⁴⁷ The device contact pads (outside of the field of view presented here and separated by $\approx 40 \,\mu\text{m}$) were connected to the nanovoltmeter via a PCB and breakout box, and the input low was connected to the microscopes ground. Figure 1(a)(i,ii) shows representations of the sideand top views of the sample, respectively. In order to stabilize skyrmions in our system, a sizable interfacial DMI is required. To meet these requirements, a perpendicular magnetic anisotropy (PMA) asymmetric multilayer comprising three repeats of a trilayer is used, including buffer and cap, where the composition was $Ta(3.2)/Pt(2.7)[Co_{68}B_{32}(0.8)/Ir(0.4)/Pt(0.6)]_{x3}/Pt(2.2)$ (thicknesses in nm). The multilayer structure was sputter deposited using an ultra-high vacuum deposition system, analogous to previously studied samples, where it was shown that Néel-type skyrmions are stabilized.1 Patterning of the multilayer was done using standard optolithography and liftoff to create a $2.3 \,\mu m$ wide microwire including the voltage contact pads required for electrical readout of thermoelectric signals. Figure 1(b) shows an atomic force micrograph detailing the topography of the microwire used in this work. Figure 1(c) shows a magnetic force micrograph and confirms the presence of singular skyrmion spin texture of ≤ 200 nm in radius. Skyrmion nucleation was achieved using the stray magnetic field from the MFM tip. 52 The corresponding zerofield scanning thermoelectric micrograph is shown in Fig. 1(d), along with line profiles in Fig. 1(e)(i,ii).

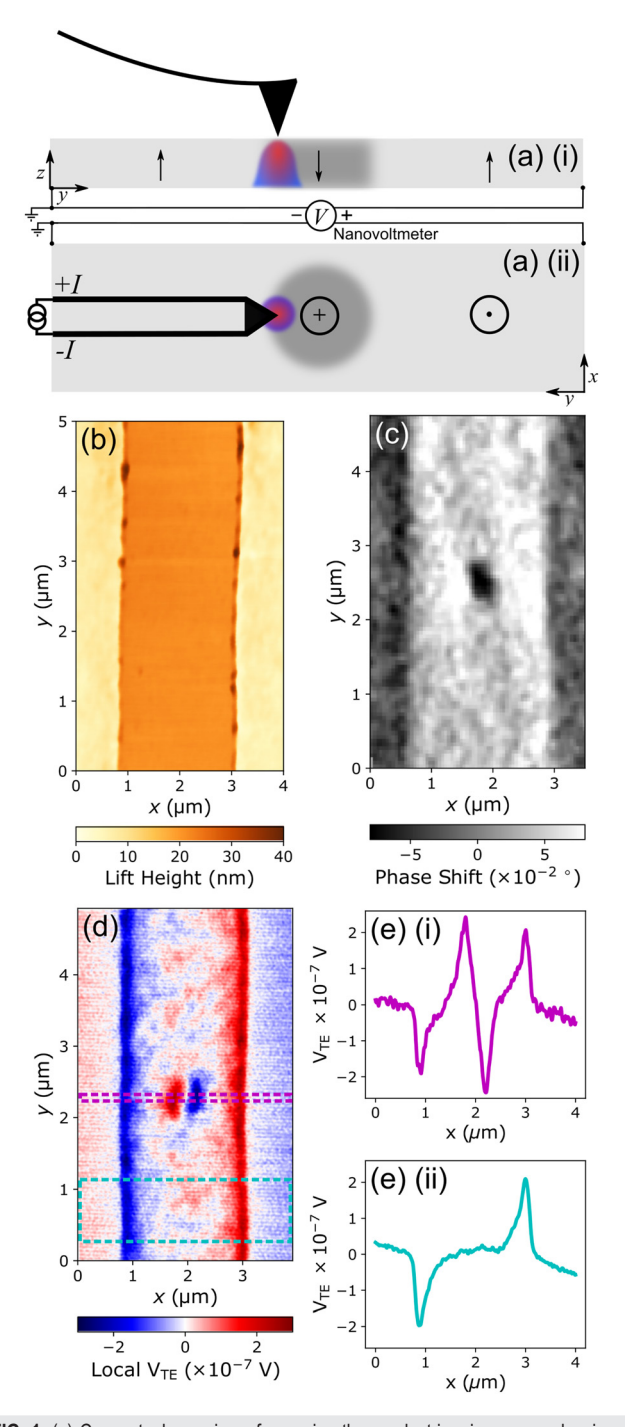


FIG. 1. (a) Conceptual overview of scanning thermoelectric microscopy, showing a schematic representation of the side(i) and top(ii) views of the device structure. Dark gray regions represent the position of the skyrmion and highlight the local projection of the z-component of magnetization. Coordinate system used for the modeling is also shown. (b) Atomic force micrograph showing the topography of the microwire. (c) Magnetic force micrograph showing a single skyrmion nucleated in the microwire. (d) Scanning thermoelectric micrograph showing the thermoelectric response from a single skyrmion, and [(e)—(i) and (ii)] averaged line profiles taken from the data in (d) from skyrmion center (i) and saturated (ii) region.

The data shown here have been treated with a simple FFT filter to remove high-frequency periodic noise, along with a 2 pixel Gaussian filter to improve the data presentation. Furthermore, the offset present in the data was removed to zero the background signal, where no thermoelectric response is expected to arise.

Here, we observe several characteristic features in the local thermoelectric response: the response from the device edges,⁴⁷ shown in Fig. 1(e)(i), and the lobe-like features that result from the skyrmion itself, Fig. 1(e)(ii), both of which are discussed in detail later. We note that the zero-field stability is likely to occur due to the attendant pinning in these multilayer material systems. Additional measurements of zero-field skyrmions in devices made of the same and similar multilayers are included in the supplementary material.

To understand the local thermoelectric response in more detail, we have modelled the response for Bloch and Néel type skyrmions. The model approximates the magnetic system as a single magnetic layer, where the spin textures have been analytically defined and constitute the input to the semi-analytical thermoelectric calculation. The thermal response to a heated tip was simulated using a custom finite difference solver,⁵³ where from previous work,⁴⁷ the temperature at the tip-sample contact point was assumed to be \approx 327 K. An example of the simulated thermal gradient, and its corresponding profile, for a simple 2-dimensional system is presented in the supplementary material. We note that it is the spatial extent of the temperature profile (the effective point spread function of the technique), which, when convolved with the magnetization texture, defines the localization of the resultant electrical field and the resolution. The electric field E that results from a thermal gradient ∇T is defined by the Seebeck tensor S through $\mathbf{E} = S\nabla \mathbf{T}$. S is constructed to contain all sources of thermoelectric response that we anticipate in our system. 54,55 It includes the anomalous Nernst effect (ANE), the anisotropic magnetothermopower (AMTP), and the planar Nernst effect (PNE).

These effects result from the asymmetry in the energy dependent scattering of electrons and holes at the Fermi level, where their differential density of states and velocities yield a net thermoelectric current, 48 which is spin polarized and interacts with the local spin texture. The ANE accounts for the transverse electric field that arises in ferromagnetic materials with spin-orbit coupling when subjected to a thermal gradient, which originates from a magnetization dependent Berry curvature and extrinsic scattering. 56-59 The AMTP and PNE account for the thermoelectric response due to spin-dependent scattering and band structure orbital anisotropy, which is highly sensitive to the angle between the local magnetization and thermal gradient⁶⁰ and occurs when $S\nabla T$ is coplanar with the local magnetization. This anisotropy is captured by the difference between the in-plane perpendicular and parallel Seebeck coefficients, $S_{\perp} \& S_{\parallel}$, respectively. Including these effects in S, Eq. (1), allows the expression for the total electric field E for an arbitrary magnetization direction to be derived. This is achieved by performing the appropriate rotation operations on S, allowing the analytical expressions of the thermoelectric response to be computed for different planes of rotation of magnetization Eq. (2), in addition to the measurement geometries. For a uniform out-of-plane magnetization, S is given by

$$S = \begin{pmatrix} S_{\perp} & -S_{N} & 0 \\ S_{N} & S_{\perp} & 0 \\ 0 & 0 & S_{\parallel} \end{pmatrix}. \tag{1}$$

In this work, we are confined to the electrical measurement along the length of the device \hat{y} , and, as stated, responses due to in-plane thermal gradients. The resulting electric field, for an arbitrary configuration, is given by

$$\mathbf{E} = S_{\perp} \nabla \mathbf{T} + (S_{\parallel} - S_{\perp})(\nabla \mathbf{T} \cdot \hat{\mathbf{m}})\hat{\mathbf{m}} - S_{N}(\hat{\mathbf{m}} \times \nabla \mathbf{T}), \tag{2}$$

where S_N is the anomalous Nernst Seebeck coefficient and $\nabla \mathbf{T}$ and $\hat{\mathbf{m}}$ are the thermal gradient and magnetization unit vector, respectively.

The voltage calculated along the length, between measurement points A and B, and across the width of the device w, is simply computed using $V_y = -\int_A^B \mathbf{E} \cdot d\mathbf{l}$. In this work, we have included only thermoelectric responses that result from in plane thermal gradients and discounted those occurring from vertical temperature differences due to the small thickness of our sample, 47,61,62 i.e., $\nabla \mathbf{T} = (\nabla T_x,$

It is important to understand the role of the balance of the inplane Seebeck coefficients as these will couple to the in-plane spin components and yield the most valuable information for fingerprinting the Bloch or Néel character of the skyrmion. Therefore, we have investigated not only the input spin texture but also the relative balance of S_{\parallel} and S_{\perp} while maintaining a fixed value for $S_N = 0.2 \,\mu\text{V} \cdot \text{K}^{-1}.^{47}$ Figures 2(a) and 2(c) show analytically defined Néel and Bloch type skyrmions, respectively, used as inputs to the thermoelectric calculation following the form. ³⁹ Figures 2(b)(i-iii) and 2(d)(i-iii) show the total thermoelectric response for the Néel and Bloch skyrmions, respectively, where in each case, (i), (ii), and (iii) correspond to S_{\perp} = -0.50, -0.75, and $-1.0 \,\mu\text{V} \cdot \text{K}^{-1}$, while for every case, S_{\parallel} was held fixed at $-1.0 \,\mu\text{V} \cdot \text{K}^{-1}$. These values are selected to approximate the resulting thermoelectric signature, focusing on the spatial response as opposed to absolute values. We demonstrate that, for lower values of S_{\perp} , when the difference between S_{\perp} and S_{\parallel} is increased, the total thermoelectric response V_{Total} is significantly different between the two spin textures [Figs. 2(b)(i) and 2(d)(i) for instance]. For the parameters simulated, the total signal is well within the sensitivity limits of the SThEM technique (\approx 15 nV). We show that, as S_{\perp} is increased, the spatial variation of V_{Total} for both the Néel and Bloch type skyrmions gradually approaches equivalence, together with a gradual decrease in the skyrmion signal amplitude due to inplane magnetization components, such that when the ratio $S_{\perp}/S_{\parallel}=1$ [Figs. 2(b)(iii) and 2(d)(iii)], there is no difference between the signals of the two spin textures. We also highlight the fact that our model additionally captures the edge response observed in the experimental data. To expound on these observations, we separate the individual thermoelectric components of $V_{\text{Total}}(\text{along } \hat{y})$ from Figs. 2(b)(i) and 2(d)(i). The relevant expressions for the ANE, PNE, and AMTP [Eqs. (3a)-(3c), respectively] are given by

$$\left[\int_{x} \frac{dx}{w(x)} \int_{y} \left[S_{N} \frac{m_{z}}{|m|} \right] \nabla T_{x}(x_{0}, y_{0}) dy, \right]$$
(3a)

$$V_{y} = \begin{cases} \int_{x} \frac{dx}{w(x)} \int_{y} \left[S_{N} \frac{m_{z}}{|m|} \right] \nabla T_{x}(x_{0}, y_{0}) dy, & (3a) \\ \int_{x} \frac{dx}{w(x)} \int_{y} \left[(S_{\parallel} - S_{\perp}) \frac{m_{x} m_{y}}{|m|^{2}} \right] \nabla T_{x}(x_{0}, y_{0}) dy, & (3b) \\ \int_{x} \frac{dx}{w(x)} \int_{y} \left[S_{\perp} \left(1 - \frac{m_{y}^{2}}{|m|^{2}} \right) + S_{\parallel} \frac{m_{y}^{2}}{|m|^{2}} \right] \nabla T_{y}(x_{0}, y_{0}) dy, & (3c) \end{cases}$$

$$\left[\int_{x} \frac{dx}{w(x)} \int_{y} \left[S_{\perp} \left(1 - \frac{m_{y}^{2}}{|m|^{2}} \right) + S_{\parallel} \frac{m_{y}^{2}}{|m|^{2}} \right] \nabla T_{y}(x_{0}, y_{0}) dy, \quad (3c)$$

where w(x) is the width of the device and x_0 and y_0 are x and y positions of the thermal probe as it is scanned during the thermoelectric

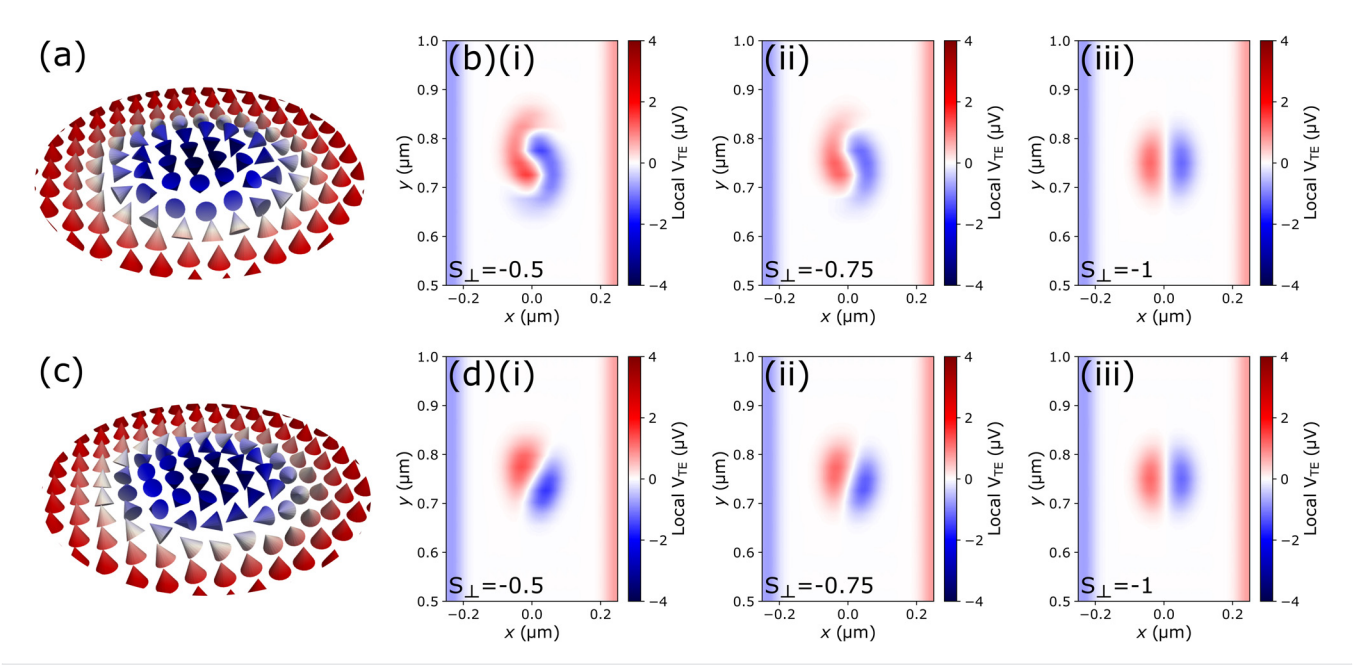


FIG. 2. Modelling of the thermoelectric response of a single skyrmion. (a) The analytically defined Néel spin texture used as the input for the thermoelectric modelling. [(b)—(i)–(iii)] The total thermoelectric response for the Néel skyrmion for $S_{\parallel}=-1.0$ and $S_{\perp}=-0.5$ (i), -0.75 (ii), and -1.0 (iii) μ V·K⁻¹. (c) and (d) Show the same for a Bloch skyrmion. (c) The analytically defined spin texture, and [(d)—(i)–(iii)] again correspond to $S_{\perp}=-0.5$ (i), -0.75 (ii), and -1.0 (iii) μ V·K⁻¹.

These expressions allow us to understand several features in the experimental and calculated data. The edge features arise purely due to the ANE [Eq. (3a)] and are a consequence of the broken symmetry of the thermal gradient at the wire edge where the integrated effect of $\nabla T_x(x_0,y_0)$ is purely positive or negative. This leads to the positive or negative signal at the device edges where $\nabla T_x(x_0,y_0)$ is opposite in sign. At the device center, there is an equal contribution such that the integrated response of $\nabla T_x(x_0,y_0)$ is nulled, and no signal results from saturated moments, as shown in Figs. 1(d), 2(b), and 2(d). We note that the gradient in the measured thermoelectric response across the device can be used to extract an estimate for the value for S_N .

Furthermore, we also observe the emergence of the ANE from the skyrmion itself, which is derived from $\nabla T_x(x_0, y_0)$ and the z-component of magnetization, which is reversed with respect to the saturated region. As such, the thermoelectric response from the skyrmion is also reversed with respect to the edge response. This is best observed in the data presented in Figs. 2(b)(iii) and 2(d)(iii), where S_{\perp} and S_{\parallel} are equal, and, therefore, only the ANE response emerges.

To understand the nuances that arise due to the spins within the skyrmion's domain wall, we plot the individual components of the thermoelectric response from Eq. (2) in Fig. 3. We show the individual thermoelectric response for the Néel and Bloch type skyrmion in Figs. 3(a) and 3(b), respectively, where in each case, (i), (ii), and (iii) are the ANE, PNE, and AMTP, respectively. The ANE is identical for both Néel and Bloch as expected, due to the same z-component for each the skyrmion type. When the in-plane spin components are considered, we see that the PNE and AMTP differ for the two skyrmion types. The PNE results in an antisymmetric multi-lobe pattern that is inverted for the two skyrmion types. This can be understood from the cyclic nature of the x and y components of the Néel and Bloch spin textures, which contribute to the $m_x m_y$ term in Eq. (3b) and lead to the inverse

relationship between the two. This cyclic response is broken for the AMTP as it solely depends on m_y ; this leads to the differing responses observed in Figs. 3(a)(iii) and 3(b)(iii). From the individual responses, we can see that their sum leads to the results presented in Fig. 2, where the PNE and AMTP act to modulate the response of the ANE for the two skyrmion types, creating two distinct sets of features in V_{Total} .

Qualitative comparison between these calculated thermoelectric responses and our experimental observations in Fig. 1(d) shows that there is a significant contribution from the ANE. Moreover, we observe a clear additional thermoelectric response from the skyrmion crosssectional profile of the experimental data, see Fig. 1(e)(i). This arises due to the additional contribution from the PNE and AMTP and, hence, contains a thermoelectric response from the wall type. The Yin-Yangesque nature of the skyrmion and the lower left (red) lobe in Fig. 1(d) suggest a Néel-like texture, where $S_{\parallel} - S_{\perp}$ is $\approx 0.25 \,\mu\text{V} \cdot \text{K}^{-1}$. However, as the measured skyrmion is not a perfect circle (magnetic inhomogeneities) and potential deviation from the idealized spin texture³⁰ due to increased magnetostatic contribution in magnetic multilayers, it is difficult to conclude with absolute certainty. Experimental measurements of the Seebeck coefficients are incredibly limited. However, recent studies on similar CoFeB/NM bilayer structures (where NM is a nonmagnetic metal known to produce DMI such as Pt, Ta, Pd etc.) have reported measurements of the spin Seebeck coefficient between $0.275-1.13 \,\mu\text{V} \cdot \text{K}^{-1}$, depending on the specific choice of NM. 63,64 This, together with the calculated anisotropy of the Seebeck coefficient of 0.1 and 0.3 $\mu V \cdot K^{-1}$ (depending on temperature and multilayer repetitions), suggests that the parameters used in the calculations are a reasonable assumption.⁶⁵ Extending this idea further, we have computed the normalized sum of fractional thermoelectric contributions from the Bloch and Néel type skyrmion spin textures. Here, we calculate the sum $V_{N\acute{e}el}x + V_{Bloch}(1-x)$ for a range of x

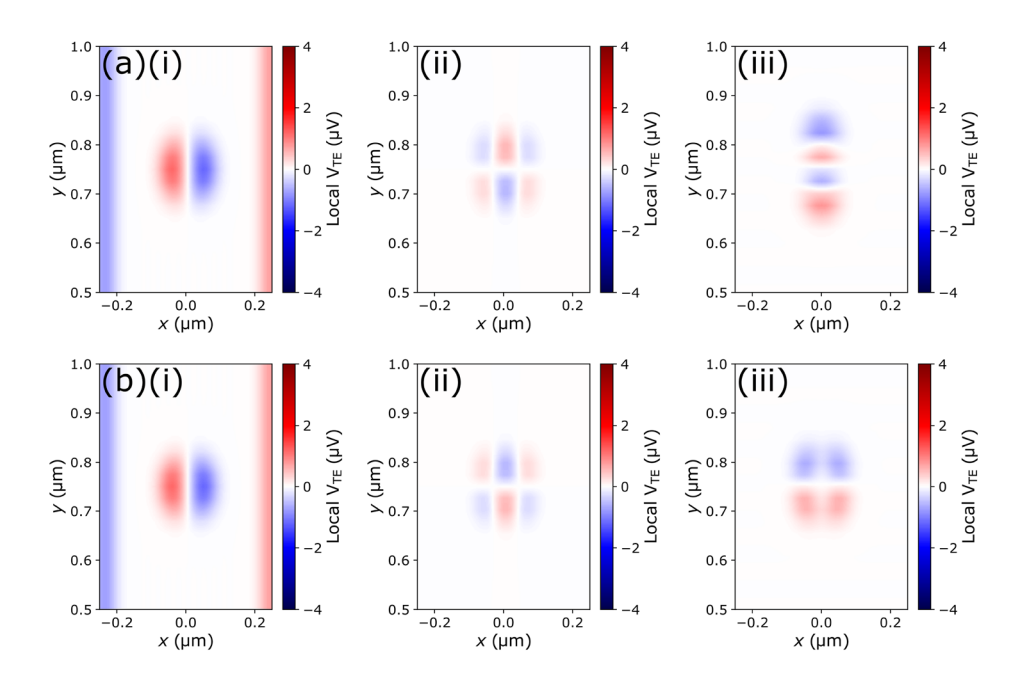


FIG. 3. Individual components of the thermoelectric response from (a) Néel and (b) Bloch skyrmion spin textures, respectively. In each case, (i)–(iii) show the individual responses from the ANE, PNE and AMTP, receptively. S_{\perp} was $-0.5\,\mu\text{V} \cdot \text{K}^{-1}$, and S_{\parallel} was $-1.0\,\mu\text{V} \cdot \text{K}^{-1}$ for all calculations.

values. Figure 4 shows the calculated normalized sum for three values of x: 0.2, 0.5, and 0.8 for (a)-(c), respectively and where $S_{\perp} = 0.5 \,\mu\text{V} \cdot \text{K}^{-1}$. Here, we demonstrate how the overall response can be tuned from Néel like to Bloch like through an average of the two spin textures when x = 0.5. This simple approach allows us to ascertain how the total V_{Total} could vary for non-ideal spin textures and demonstrates how a mixed state could approximate the experimental data. We note that our stack comprises three trilayers and, therefore, is below the typical repetition number³⁰ for magnetostatics to lead to hybrid skyrmion textures. Therefore, we propose that an alternative explanation is that $S_{\parallel} - S_{\perp}$ is small but non-negligible. In this scenario, the difference is such that the peak contribution from the skyrmion domain wall is detectable within the sensitivity limits of the technique, as demonstrated in line profile through the experimental data, Fig. 1(e)(i). However, the spatial extent and the tails present in the Néel skyrmion, Fig. 2(b)(ii), are such that they are below the detection limit of the measurement, reducing the distinguishability in this case. This represents an interesting avenue to explore in future work. Scanning thermoelectric microscopy could be performed on thin lamellae of B20 crystals or 2D ferromagnets, which have been shown to be room-temperature or near-room-temperature Bloch skyrmion hosts. 66,67 Additionally, the results presented in Fig. 4 could be used to interpret skyrmions in large-repetition multilayers, where it has been shown that skyrmions possess mixed Bloch-Neel characteristics.³⁰

Nevertheless, our modelling shows that SThEM is a powerful technique for fingerprinting magnetic spin textures and has the potential to reveal the Néel or Bloch nature of individual skyrmions using a simple laboratory setup. We suggest that it would be best applied to ideal spin textures, such as those found in two-dimensional ferromagnets (pure spin textures), and for materials systems where S_{\perp} and S_{\parallel} are significantly different, increasing the signal-to-noise ratio. The inspection of Eqs. (2) and (3) shows that because the $m_x m_y$ product is the same in either case, it is not possible to determine the helicity from SThM alone. Similarly, it was shown that it was not possible to

measure the chirality of Néel walls with this technique for the same reason. The wall analysis can easily be combined with MFM, often in the same microscope setup. It has been shown that, with MFM, the helicity of skyrmions can be determined, making the combination of these techniques ideal for fast characterization of spin textures. Finally, although considering the TE response due to in-plane thermal gradients captures the experimentally measured data well, it is conceivable that the vertical gradient could yield additional information. Indeed, our Seebeck tensor already reveals this relationship for the effects and experimental geometry considered here. Therefore, we anticipate that future work would involve accounting for any potential contribution due to ∇T_z and subsequent modification of the Seebeck tensor to account for additional effects such as the spin Seebeck effect (SSE)—particularly important for insulating magnetic samples.

To conclude, we have used SThEM to measure the local thermoelectric response from a single skyrmion when interrogated with a highly localized thermal gradient. The resultant thermoelectric response is the sum of the individual components from all thermally driven spin-dependent transport phenomena. These are included in the Seebeck tensor, which is used to derive various expressions for the individual thermoelectric voltages. Therefore, the measured voltage is directly linked to the underlying spin structure of the skyrmion. Through additional thermoelectric modelling, we show that it is possible to fingerprint skyrmion types, Bloch and Néel, due to the unique thermoelectric responses resulting from their differing underlying spin textures. The extent to which their spin textures can be distinguished is explored by varying the relative size of the in-plane Seebeck coefficients, S_{\perp} and S_{\parallel} , which is material dependent. Our study demonstrates how a simple atomic force microscope can be harnessed to explore the underlying magnetization of topological spin textures. We further suggest, based on our best-case measurement noise floor of \approx 15 nV, that this methodology could be employed to also explore thermally driven topological signatures in the measured data. The combination of high sensitivity and position-control of the stimulus in such proximity to the spin

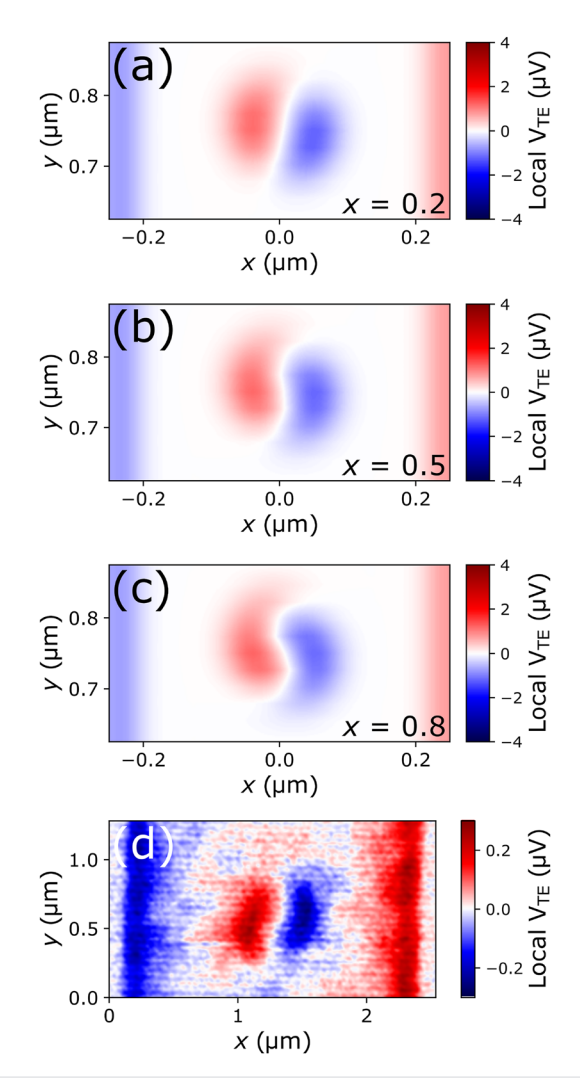


FIG. 4. Combined Bloch and Néel thermoelectric responses, showing the normalized sum for a varying ratio of Bloch to Néel magnetization configuration $V_{N\acute{e}el}X + V_{Bloch}(1-x)$ for (a) x=0.2, (b) x=0.5, and (c) x=0.8. Panel (d) shows a zoom in of the experimental data from Fig. 1(d) for comparison.

texture could create a fruitful playground for highly localized investigations of topological phenomena. Our work will open a route to nanoscale optimization of skyrmion-based spin caloritronic materials and devices, accelerating existing technology readiness, and additionally driving progress in the next generation of devices where thermally driven topological phenomena will play a central role.

See the <u>supplementary material</u> for additional scanning thermoelectric microscopy images of zero-field skyrmions in devices fabricated from both identical and similar multilayers and example calculated thermal gradient used in the modelling of the thermoelectric response.

This work was supported in part by the European Metrology Research Programme (EMRP) and EMRP participating countries under the European Metrology Programme for Innovation and Research (EMPIR) under Project No. 17FUN08 TOPS: Metrology for topological spin structures. The project also received financial support from the UK government department for Science, Innovation and Technology through NMS funding (Metrology of complex systems for low energy computation). Financial support was also received through the PID2022-137567NB-C21/AEI/ 10.13039/501100011033 grant from the Spanish Ministry of Science and Innovation. Further support was also received through European Union Horizon 2020 funding scheme–(H2020 Grant MAGicSky No. FET-Open-665095.103).

AUTHOR DECLARATIONS Conflict of Interest

The authors have no conflicts to disclose.

Author Contributions

Christopher E. A. Barker: Conceptualization (equal); Formal analysis (equal); Methodology (equal); Writing - original draft (lead); Writing - review & editing (equal). Elias Saugar: Conceptualization (equal); Formal analysis (equal); Methodology (equal); Writing - review & editing (equal). Katharina Zeissler: Conceptualization (supporting); Formal analysis (supporting); Methodology (supporting); Writing review & editing (equal). Robert Puttock: Conceptualization (supporting); Formal analysis (supporting); Methodology (supporting); Writing - review & editing (equal). Petr Klapetek: Conceptualization (supporting); Formal analysis (supporting); Methodology (supporting); Writing - review & editing (equal). Olga Kazakova: Conceptualization (supporting); Formal analysis (supporting); Methodology (supporting); Writing - review & editing (equal). Christopher H. Marrows: Conceptualization (supporting); Formal analysis (supporting); Methodology (supporting); Supervision (lead); Writing - review & editing (equal). Oksana Chubykalo-Fesenko: Conceptualization (lead); Formal analysis (lead); Funding acquisition (lead); Methodology (equal); Supervision (lead); Writing - review & editing (equal). Craig Barton: Conceptualization (lead); Formal analysis (lead); Funding acquisition (lead); Methodology (lead); Project administration (lead); Supervision (lead); Writing - original draft (lead); Writing – review & editing (equal).

DATA AVAILABILITY

The data that support the findings of this study are openly available in Research Data Leeds at https://doi.org/10.5518/1763.

REFERENCES

- ¹I. Dzyaloshinskii, "Theory of helicoidal structures in antiferromagnets," Sov. Phys. JETP **20**, 665 (1965).
- ²A. Bogdanov and D. A. Yablonskii, "Thermodynamically stable vortices in magnetically ordered crystals. The mixed state of magnets," Sov. Phys. JETP 88, 101–103 (1989).
- ³W. Jiang, W. Zhang, G. Yu, M. B. Jungfleisch, P. Upadhyaya, H. Somaily, J. E. Pearson, Y. Tserkovnyak, K. L. Wang, O. Heinonen, S. G. E. te Velthuis, and A. Hoffmann, "Mobile Néel skyrmions at room temperature: Status and future," AIP Adv. 6, 055602 (2016).
- ⁴N. Nagaosa and Y. Tokura, "Topological properties and dynamics of magnetic skyrmions," Nat. Nanotechnol. **8**, 899–911 (2013).

- ⁵R. Wiesendanger, "Nanoscale magnetic skyrmions in metallic films and multilayers: A new twist for spintronics," Nat. Rev. Mater. 1, 1–11 (2016).
- ⁶A. Fert, N. Reyren, and V. Cros, "Advances in the physics of magnetic skyrmions and perspective for technology," Nat. Mater. 2, 17031 (2017).
- ⁷K. Everschor-Sitte, J. Masell, R. M. Reeve, and M. Kläui, "Perspective: Magnetic skyrmions—overview of recent progress in an active research field," J. Appl. Phys. 124, 240901 (2018).
- ⁸X. Zhang, Y. Zhou, K. Mee Song, T.-E. Park, J. Xia, M. Ezawa, X. Liu, W. Zhao, G. Zhao, and S. Woo, "Skyrmion-electronics: Writing, deleting, reading and processing magnetic skyrmions toward spintronic applications," J. Phys. Condens. Matter 32, 143001 (2020).
- ⁹B. Göbel, I. Mertig, and O. A. Tretiakov, "Beyond skyrmions: Review and perspectives of alternative magnetic quasiparticles," Phys. Rep. 895, 1–28 (2021).
- ¹⁰N. Romming, A. Kubetzka, C. Hanneken, K. von Bergmann, and R. Wiesendanger, "Field-dependent size and shape of single magnetic skyrmions," Phys. Rev. Lett. 114, 177203 (2015).
- ¹¹S. Meyer, M. Perini, S. Malottki, A. Kubetzka, R. Wiesendanger, K. von Bergmann, and S. Heinze, "Isolated zero field sub-10 nm skyrmions in ultrathin co films," Nat. Commun. 10, 3823 (2019).
- ¹²L. Caretta, M. Mann, F. Büttner, K. Ueda, B. Pfau, C. Günther, P. Hessing, A. Churikova, C. Klose, M. Schneider, D. Engel, C. Marcus, D. Bono, K. Bagschik, S. Eisebitt, and G. Beach, "Fast current-driven domain walls and small skyrmions in a compensated ferrimagnet," Nat. Nanotechnol. 13, 1154 (2018).
- ¹³K. Hamamoto, M. Ezawa, and N. Nagaosa, "Quantized topological Hall effect in skyrmion crystal," Phys. Rev. B 92, 115417 (2015).
- ¹⁴H. Wang, Y. Dai, G.-M. Chow, and J. Chen, "Topological Hall transport: Materials, mechanisms and potential applications," Prog. Mater. Sci. 130, 100971 (2022).
- ¹⁵W. Jiang, X. Zhang, G. Yu, W. Zhang, M. Jungfleisch, J. Pearson, O. Heinonen, K. Wang, Y. Zhou, A. Hoffmann, and S. Velthuis, "Direct observation of the skyrmion Hall effect," Nat. Phys. 13, 162 (2017).
- ¹⁶W. Legrand, D. Maccariello, N. Reyren, K. Garcia, C. Moutafis, C. Moreau-Luchaire, S. Collin, K. Bouzehouane, V. Cros, and F. Albert, "Room-temperature current-induced generation and motion of sub-100 nm skyrmions," Nano Lett. 17, 2703–2712 (2017).
- ¹⁷R. Juge, S.-G. Je, D. S. Chaves, L. D. Buda-Prejbeanu, J. Peña Garcia, J. Nath, I. M. Miron, K. G. Rana, L. Aballe, M. Foerster, F. Genuzio, T. O. Mentes, A. Locatelli, F. Maccherozzi, S. S. Dhesi, M. Belmeguenai, Y. Roussigné, S. Auffret, S. Pizzini, G. Gaudin, J. Vogel, and O. Boulle, "Current-driven skyrmion dynamics and drive-dependent skyrmion Hall effect in an ultrathin film," Phys. Rev. Appl. 12, 044007 (2019).
- ¹⁸K. Zeissler, S. Finizio, C. Barton, A. Huxtable, J. Massey, J. Raabe, A. Sadovnikov, S. Nikitov, R. Brearton, T. Hesjedal, G. Laan, M. Rosamond, E. Linfield, G. Burnell, and C. Marrows, "Diameter-independent skyrmion Hall angle observed in chiral magnetic multilayers," Nat. Commun. 11, 428 (2020).
- ¹⁹K. Litzius, J. Leliaert, P. Bassirian, D. Rodrigues, S. Kromin, I. Lemesh, J. Zázvorka, K. J. Lee, J. Mulkers, N. Kerber, D. Heinze, N. Keil, R. Reeve, M. Weigand, B. Waeyenberge, G. Schütz, K. Everschor-Sitte, G. Beach, and M. Kläui, "The role of temperature and drive current in skyrmion dynamics," Nat. Electron. 3, 30–36 (2020).
- ²⁰K. Wang, V. Bheemarasetty, J. Duan, S. Zhou, and G. Xiao, "Fundamental physics and applications of skyrmions: A review," J. Magn. Magn. Mater. 563, 169905 (2022).
- ²¹O. Lee, R. Msiska, M. A. Brems, M. Kläui, H. Kurebayashi, and K. Everschor-Sitte, "Perspective on unconventional computing using magnetic skyrmions," Appl. Phys. Lett. 122, 260501 (2023).
- ²²R. Zhu, Z. Jiang, X. Zhang, X. Zhong, C. Tan, M. Liu, Y. Sun, X. Li, R. Qi, K. Qu, Z. Liu, M. Wu, M. Li, B. Huang, Z. Xu, J. Wang, K. Liu, P. Gao, J. Wang, J. Li, and X. Bai, "Dynamics of polar skyrmion bubbles under electric fields," Phys. Rev. Lett. 129, 107601 (2022).
- ²³F. Büttner, I. Lemesh, M. Schneider, B. Pfau, C. Günther, P. Hessing, J. Geilhufe, L. Caretta, D. Engel, B. Krüger, J. Viefhaus, S. Eisebitt, and G. Beach, "Field-free deterministic ultra fast creation of skyrmions by spin orbit torques," Nat. Nanotechnol. 12, 1040–1044 (2017).
- ²⁴X. Yu, F. Kagawa, S. Seki, M. Kubota, J. Masell, F. Yasin, K. Nakajima, M. Nakamura, M. Kawasaki, N. Nagaosa, and Y. Tokura, "Real-space observations

- of 60-nm skyrmion dynamics in an insulating magnet under low heat flow," Nat. Commun. 12, 5079 (2021).
- ²⁵C. Gong, Y. Zhou, and G. Zhao, "Dynamics of magnetic skyrmions under temperature gradients," Appl. Phys. Lett. 120, 052402 (2022).
- 26A. Fernández Scarioni, C. Barton, H. Corte-León, S. Sievers, X. Hu, F. Ajejas, W. Legrand, N. Reyren, V. Cros, O. Kazakova, and H. W. Schumacher, "Thermoelectric signature of individual skyrmions," Phys. Rev. Lett. 126, 077202 (2021).
- ²⁷Z. Li, M. Ma, Z. Chen, K. Xie, and F. Ma, "Interaction between magnon and skyrmion: Toward quantum magnonics," J. Appl. Phys. 132, 210702 (2022).
- ²⁸S. Mcvitie, S. Hughes, K. Fallon, S. McFadzean, D. McGrouther, M. Krajnak, W. Legrand, D. Maccariello, S. Collin, K. Garcia, N. Reyren, V. Cros, A. Fert, K. Zeissler, and C. Marrows, "A transmission electron microscope study of Néel skyrmion magnetic textures in multilayer thin film systems with large interfacial chiral interaction," Sci. Rep. 8, 5703 (2018).
- ²⁹Y. Dovzhenko, F. Casola, S. Schlotter, T. Zhou, F. Büttner, R. Walsworth, G. Beach, and A. Yacoby, "Magnetostatic twists in room-temperature skyrmions explored by nitrogen-vacancy center spin texture reconstruction," Nat. Commun. 9, 2712 (2018).
- ³⁰W. Legrand, J.-Y. Chauleau, D. Maccariello, N. Reyren, S. Collin, K. Bouzehouane, N. Jaouen, V. Cros, and A. Fert, "Hybrid chiral domain walls and skyrmions in magnetic multilayers," Sci. Adv. 4, 0415 (2018).
- Gross, W. Akhtar, A. Hrabec, J. Sampaio, L. J. Martínez, S. Chouaieb, B. J. Shields, P. Maletinsky, A. Thiaville, S. Rohart, and V. Jacques, "Skyrmion morphology in ultrathin magnetic films," Phys. Rev. Mater. 2, 024406 (2018).
 A. Finco, A. Haykal, R. Tanos, F. Fabre, S. Chouaieb, W. Akhtar, I. Robert-
- ³²A. Finco, A. Haykal, R. Tanos, F. Fabre, S. Chouaieb, W. Akhtar, I. Robert-Philip, W. Legrand, F. Ajejas, K. Bouzehouane, N. Reyren, T. Devolder, J.-P. Adam, J.-V. Kim, V. Cros, and V. Jacques, "Imaging non-collinear antiferromagnetic textures via single spin relaxometry," Nat. Commun. 12, 767 (2021).
- ³³C. Donnelly, S. Gliga, V. Scagnoli, M. Holler, J. Raabe, L. J. Heyderman, and M. Guizar-Sicairos, "Tomographic reconstruction of a three-dimensional magnetization vector field," New J. Phys. 20, 083009 (2018).
- ³⁴C. Donnelly, S. Finizio, S. Gliga, M. Holler, A. Hrabec, M. Kronenberg, S. Mayr, V. Scagnoli, L. Heyderman, M. Guizar-Sicairos, and J. Raabe, "Time-resolved imaging of three-dimensional nanoscale magnetization dynamics," Nat. Nanotechnol. 15, 356 (2020).
- 35H. J. Hug, B. Stiefel, P. J. A. van Schendel, A. Moser, R. Hofer, S. Martin, H.-J. Güntherodt, S. Porthun, L. Abelmann, J. C. Lodder, G. Bochi, and R. C. O'Handley, "Quantitative magnetic force microscopy on perpendicularly magnetized samples," J. Appl. Phys. 83, 5609–5620 (1998).
- ³⁶P. J. A. van Schendel, H. J. Hug, B. Stiefel, S. Martin, and H.-J. Güntherodt, "A method for the calibration of magnetic force microscopy tips," J. Appl. Phys. 88, 435–445 (2000).
- ³⁷M. Baćani, M. Marioni, J. Schwenk, and H. Hug, "How to measure the local Dzyaloshinskii Moriya interaction in skyrmion thin film multilayers," Sci. Rep. 9, 3114 (2019).
- ³⁸A. Yagil, A. Almoalem, A. Soumyanarayanan, A. K. C. Tan, M. Raju, C. Panagopoulos, and O. M. Auslaender, "Stray field signatures of Néel textured skyrmions in Ir/Fe/Co/Pt multilayer films," Appl. Phys. Lett. 112, 192403 (2018).
- ³⁹C. Barton, A. Fernández Scarioni, B. Sakar, S. Sievers, F. Garcia-Sanchez, P. Thompson, F. Ajejas, W. Legrand, N. Reyren, T. Thomson, V. Cros, H. W. Schumacher, and O. Kazakova, "Radially dependent stray field signature of chiral magnetic skyrmions," Phys. Rev. B 108, 104409 (2023).
- ⁴⁰J. Bartell, D. Ngai, Z. Leng, and G. Fuchs, "Towards a table-top microscope for nanoscale magnetic imaging using picosecond thermal gradients," Nat. Commun. 6, 8460 (2015).
- ⁴¹E. Pfitzner, X. Hu, H. W. Schumacher, A. Hoehl, D. Venkateshvaran, M. Cubukcu, J.-W. Liao, S. Auffret, J. Heberle, J. Wunderlich, and B. Kästner, "Near-field magneto-caloritronic nanoscopy on ferromagnetic nanostructures," AIP Adv. 8, 125329 (2018).
- ⁴²R. Iguchi, S. Kasai, K. Koshikawa, N. Chinone, S. Suzuki, and K. Uchida, "Thermoelectric microscopy of magnetic skyrmions," Sci. Rep. 9, 18443 (2019).
- ⁴³I. Gray, G. M. Stiehl, J. T. Heron, A. B. Mei, D. G. Schlom, R. Ramesh, D. C. Ralph, and G. D. Fuchs, "Imaging uncompensated moments and exchange-biased emergent ferromagnetism in FeRh thin films," Phys. Rev. Mater. 3, 124407 (2019).

- ⁴⁴T. Janda, J. Godinho, T. Ostatnicky, E. Pfitzner, G. Ulrich, A. Hoehl, S. Reimers, Z. Šobáň, T. Metzger, H. Reichlová, V. Novák, R. P. Campion, J. Heberle, P. Wadley, K. W. Edmonds, O. J. Amin, J. S. Chauhan, S. S. Dhesi, F. Maccherozzi, R. M. Otxoa, P. E. Roy, K. Olejník, P. Němec, T. Jungwirth, B. Kaestner, and J. Wunderlich, "Magneto-Seebeck microscopy of domain switching in collinear antiferromagnet CuMnAs," Phys. Rev. Mater. 4, 094413 (2020).
- 45 A. Sola, C. Barton, V. Basso, C. Dubs, M. Pasquale, and O. Kazakova, "Local spin Seebeck imaging with a scanning probe," Phys. Rev. Appl. 14, 034056 (2020).
- ⁴⁶A. Harzheim, C. Evangeli, O. V. Kolosov, and P. Gehring, "Direct mapping of local Seebeck coefficient in 2D material nanostructures via scanning thermal gate microscopy," 2D Mater. 7, 041004 (2020).
- 47R. Puttock, C. Barton, E. Saugar, P. Klapetek, A. Fernández-Scarioni, P. Freitas, H. W. Schumacher, T. Ostler, O. Chubykalo-Fesenko, and O. Kazakova, "Local thermoelectric response from a single Néel domain wall," Sci. Adv. 8, eadc9798 (2022)
- 48G. Bauer, E. Saitoh, and B. Wees, "Spin caloritronics," Nat. Mater. 11, 391–399 (2012).
- ⁴⁹S. R. Boona, R. C. Myers, and J. P. Heremans, "Spin caloritronics," Energy Environ. Sci. 7, 885–910 (2014).
- ⁵⁰H. Yu, S. D. Brechet, and J.-P. Ansermet, "Spin caloritronics, origin and outlook," Phys. Lett. A 381, 825–837 (2017).
- ⁵¹S. Finizio, K. Zeissler, S. Wintz, S. Mayr, T. Weßels, A. J. Huxtable, G. Burnell, C. H. Marrows, and J. Raabe, "Deterministic field-free skyrmion nucleation at a nanoengineered injector device," Nano Lett. 19, 7246–7255 (2019).
- ⁵²C. E. A. Barker, K. Zeiesler, E. Jeffery, F. Garcia-Sanchez, J.-V. Kim, G. Burnell, O. Kazakova, C. H. Marrows, and C. Barton, "Domain wall enhanced skyrmion motion" (unpublished) (2025).
- ⁵³P. Klapetek, J. Martinek, P. Grolich, M. Valtr, and N. Kaur, "Graphics cards based topography artefacts simulations in scanning thermal microscopy," Int. J. Heat Mass Transfer 108, 841–850 (2017).
- ⁵⁴O. Reimer, D. Carsten, M. Bovender, L. Helmich, J.-O. Dreessen, J. Krieft, A. Shestakov, C. Back, J.-M. Schmalhorst, A. Hutten, G. Reiss, and T. Kuschel, "Quantitative separation of the anisotropic magnetothermopower and planar Nernst effect by the rotation of an in-plane thermal gradient," Sci. Rep. 7, 40586 (2017).
- 55P. Krzysteczko, J. Wells, A. Fernández Scarioni, Z. Soban, T. Janda, X. Hu, V. Saidl, R. P. Campion, R. Mansell, J.-H. Lee, R. P. Cowburn, P. Nemec,

- O. Kazakova, J. Wunderlich, and H. W. Schumacher, "Nanoscale thermoelectrical detection of magnetic domain wall propagation," Phys. Rev. B **95**, 220410 (2017).
- 56 J. Smit, "The spontaneous Hall effect in ferromagnetics I," Physica 21, 877–887 (1955).
- 57L. Berger, "Side-jump mechanism for the Hall effect of ferromagnets," Phys. Rev. B 2, 4559–4566 (1970).
- ⁵⁸M. V. Berry, "Quantal phase factors accompanying adiabatic changes," Proc. R. Soc. London A 392, 45–57 (1984).
- ⁵⁹N. Nagaosa, J. Sinova, S. Onoda, A. H. MacDonald, and N. P. Ong, "Anomalous Hall effect," Rev. Mod. Phys. 82, 1539–1592 (2010).
- ⁶⁰I. A. Campbell, "Hall effect and resistivity anisotropy in Ni alloys," Phys. Rev. Lett. 24, 269–271 (1970).
- ⁶¹K. Uchida, S. Takahashi, K. Harii, J. Ieda, W. Koshibae, K. Ando, S. Maekawa, and E. Saitoh, "Observation of the spin Seebeck effect," Nature 455, 778–781 (2008)
- ⁶²H. Adachi, K. Uchida, E. Saitoh, and S. Maekawa, "Theory of the spin Seebeck effect," Rep. Prog. Phys. **76**, 036501 (2013).
- ⁶³K.-D. Lee, D.-J. Kim, H. Yeon Lee, S.-H. Kim, J.-H. Lee, K.-M. Lee, J.-R. Jeong, K.-S. Lee, H.-S. Song, J.-W. Sohn, S.-C. Shin, and B.-G. Park, "Thermoelectric signal enhancement by reconciling the spin Seebeck and anomalous Nernst effects in ferromagnet/non-magnet multilayers," Sci. Rep. 5, 10249 (2015).
- ⁶⁴M. Gamino, J. S. Santos, A. R. Souza, A. Melo, R. Della Pace, E. Silva, A. Oliveira, R. Rodríguez-Suárez, F. Bohn, and M. Correa, "Longitudinal spin Seebeck effect and anomalous Nernst effect in CoFeB/non-magnetic metal bilayers," J. Magn. Magn. Mater. 527, 167778 (2021).
- 65 V. Popescu and P. Kratzer, "Large Seebeck magnetic anisotropy in thin Co films embedded in Cu determined by *ab initio* investigations," Phys. Rev. B 88, 104425 (2013).
- ⁶⁶A. C. Twitchett-Harrison, J. C. Loudon, R. A. Pepper, M. T. Birch, H. Fangohr, P. A. Midgley, G. Balakrishnan, and P. D. Hatton, "Confinement of skyrmions in nanoscale fege device-like structures," ACS Appl. Electron. Mater. 4, 4427–4437 (2022).
- ⁶⁷X. Lv, H. Lv, Y. Huang, R. Zhang, G. Qin, Y. Dong, M. Liu, K. Pei, G. Cao, J. Zhang, Y. Lai, and R. Che, "Distinct skyrmion phases at room temperature in two-dimensional ferromagnet Fe₃GaTe₂," Nat. Commun. 15, 3278 (2024).